

Statistical fluctuations of pumping and rectification currents in quantum dots

M. Martínez-Mares and C. H. Lewenkopf

*Instituto de Física, Universidade do Estado do Rio de Janeiro,
R. São Francisco Xavier 524, 20550-900 Rio de Janeiro, Brazil*

E. R. Mucciolo

Department of Physics, Duke University, Durham, North Carolina 27708

Departamento de Física, Pontifícia Universidade Católica do Rio de Janeiro, C.P. 38071, 22452-970 Rio de Janeiro, Brazil

(Dated: October 30, 2018)

We investigate the statistical fluctuations of currents in chaotic quantum dots induced by pumping and rectification at finite temperature and in the presence of dephasing. In open quantum dots, dc currents can be generated by the action of two equal-frequency ac gate voltages. The adiabatic regime occurs when the driving frequency is smaller than the electron inverse dwell time. Using numerical simulations complemented by semiclassical calculations, we consider both limits of small and large number of propagating channels in the leads when time-reversal symmetry is fully broken. We find that at intermediate temperature regimes, namely, $k_B T \lesssim \Delta$, where Δ is the mean single-particle level spacing, thermal smearing suppresses the current amplitude more effectively than dephasing. Motivated by recent theoretical and experimental works, we also study the statistics of rectified currents in the presence of a parallel, Zeeman splitting, magnetic field.

PACS numbers: 73.21.La, 73.23.-b, 72.25.Dc

I. INTRODUCTION

The study of non-equilibrium transport phenomena in mesoscopic electronic systems has attracted much attention in recent years, in particular for ballistic quantum dots formed in semiconductor heterostructures. Besides the investigation of non-linear $I - V$ characteristics, it has been proposed that dc currents can be induced by the simultaneous application of two ac, shape-deforming gate voltages, the so-called pumping effect.^{1,2,3,4} An experimental realization of an adiabatic quantum dot pump of electrons under these conditions has been reported.⁵ For open quantum dots, where the system is connected to reservoirs by one or more propagating channels at each contact, the pumping current has usually both pure quantum (dissipationless) and rectified (dissipative) components.⁶ While attempts have been made to maximize the former, it seems that current experiments are still dominated by the latter. Nevertheless, the effects of phase coherence can also be present in the rectified component. A clear indication of that has been given by the observation of a mesoscopic spin current⁷ by Watson *et al.*⁸ in a setup where most likely rectification is still the primary source of pumping.

In electronic mesoscopic systems, phase coherence and the consequent lack of self-averaging are responsible for the sample-to-sample fluctuations of most transport properties. For systems with an underlying chaotic dynamics, these fluctuations are characterized by universal statistics. Therefore, for either quantum pumping or rectification, it is important to understand what are the universal features of current fluctuations. Being universal, these features can be described, in principle, by a theory based only on a few hypotheses about the system symmetries and its connection to the reservoirs and

the environment. In fact, by comparing universal probability distributions and correlation functions with actual experimental measurements, one may be able to gain information about nonuniversal effects. Also, through this procedure, it might be possible to estimate the amplitude of phase decoherence present in the device.

The theory of zero-temperature statistical properties of the pumping current in quantum dots³ explains qualitatively several aspects of the experiment.⁵ A quantitative approach, however, requires treating both temperature and the consequent dephasing effects. Previous work addressing dephasing did not account for the thermal rounding of the Fermi surface.^{9,10} Albeit the thermal convolution for the pumping current being casted in a very simple expression, assessing the fluctuations requires the computation of nontrivial energy correlation functions. These correlation functions were calculated only in the absence of dephasing and when a large number of propagating channels ($N \gg 1$) is present.^{11,12} In this limiting case, the role of temperature is well understood. In the present work we use analytical and numerical calculations to study the effects of temperature and dephasing in the case of small number of channels $N \geq 2$, which is more relevant to the experiments. Also, we revisit the case of $N \gg 1$ from a semiclassical viewpoint, where results can be obtained in a more transparent and insightful way than from the diagrammatic technique.

The paper is organized as follows. In Sec. II, we briefly present the general theory of pumping currents in open QDs in the adiabatic regime. Finite-temperature pumping current fluctuations are expressed as integrals over correlation functions of scattering matrices in Sec. II A. In Sec. II B, we show that such correlation functions are readily calculated by means of the semiclassical approximation. The small- N limit is investigated numerically in

Sec. II C. The combined effect of dephasing and temperature is discussed in Sec. II D. In Sec. III we address the influence of capacitive couplings on the pumping currents and their rectification effects. Mesoscopic fluctuations of spin pumping currents are discussed in Sec. IV. Finally, in Sec. V, we present our conclusions.

II. PUMPING CURRENTS

We consider a quantum dot (QD) formed by laterally confining a region of a two-dimensional electron gas (2DEG) through multiple electrostatic gate voltages. The electrons in the QD have free access to the rest of the 2DEG through two point-contact leads. We assume that the “right” and “left” leads support N_R and N_L fully transmitting modes, respectively. The confining potential of the QD undergoes a periodic shape deformation caused by the ac modulation of two gate voltages, which can be parameterized by $X_1(t) = a_1 \cos(\omega t + \phi_1)$ and $X_2(t) = a_2 \cos(\omega t + \phi_2)$. Here, ω denotes the driving frequency, $\phi = \phi_2 - \phi_1$ is the (constant) phase difference between voltages, and a_1 and a_2 are their amplitudes. We focus our treatment of the problem to the adiabatic regime, when the driving frequency of the perturbations is much smaller than the electron escape rate (or inverse dwell time): $\omega \ll \Gamma/\hbar = N\Delta/2\pi\hbar$, where $N = N_R + N_L$ and Δ is the mean level spacing in the QD when isolated from the reservoirs.

The adiabatic deformations of the QD confining potential induce charge transfer through the point contacts. In the linear response limit, the amount of charge passing through a given contact l ($l = L, R$) is expressed as¹³

$$\delta Q_l = e \left(\frac{dn_l}{dX_1} \delta X_1 + \frac{dn_l}{dX_2} \delta X_2 \right), \quad (1)$$

where the so-called emissivities can be written in terms of scattering matrix elements, namely,

$$\frac{dn_l}{dX_i} = \frac{1}{2\pi} \sum_{\beta} \sum_{\alpha \in l} \text{Im} \left(\frac{\partial S_{\alpha\beta}}{\partial X_i} S_{\alpha\beta}^* \right), \quad (2)$$

for $i = 1, 2$. Thus, the total charge per cycle transferred through the contact l can be evaluated by integrating Eq. (1) over one period,

$$Q_l = e \int_0^{2\pi/\omega} dt \left[\frac{dn_l}{dX_1} \frac{dX_1}{dt} + \frac{dn_l}{dX_2} \frac{dX_2}{dt} \right]. \quad (3)$$

One can use Eqs. (2), (3), and rewrite the integral over time as an integral over the surface area \mathcal{A} swept by X_1 and X_2 in parameter space over one period. Moreover, it is not difficult to prove that $Q_L = -Q_R$, since charge is not accumulated inside the QD (see below). As a result, we can cast the zero temperature pumping current going from left to right reservoirs as³

$$I_0(E_F) = \frac{\omega Q_L}{2\pi} = \frac{e\omega}{2\pi} \int_{\mathcal{A}} dX_1 dX_2 \Pi_0^L(E_F, \mathbf{X}), \quad (4)$$

where $\mathbf{X} = (X_1, X_2)$. Notice that only electrons in states at the Fermi energy contribute to the current (we have used the subscript in the current to indicate temperature). In terms of the S matrix, the pumping response function Π_0^l reads

$$\Pi_0^l(E, \mathbf{X}) = \frac{1}{\pi} \sum_{\beta} \sum_{\alpha \in l} \text{Im} \left(\frac{\partial S_{\alpha\beta}^*}{\partial X_1} \frac{\partial S_{\alpha\beta}}{\partial X_2} \right). \quad (5)$$

The energy and parameter dependences of the response function are determined by those of the scattering matrix. Therefore, it is necessary to make an explicit connection between the latter and the microscopic details of the system. Such connection is provided by¹⁴

$$S(E, \mathbf{X}) = \mathbb{1} - 2i\pi W^\dagger \frac{1}{E - H(\mathbf{X}) + i\pi W W^\dagger} W, \quad (6)$$

where E is the energy of incoming and outgoing electrons (assuming that no bias voltage is applied to the system). W is a $M \times N$ matrix that gives the coupling between the M resonant single-particle electronic states in the QD, described by the $M \times M$ Hamiltonian matrix $H(\mathbf{X})$, and the N propagating modes in the leads.

Throughout this paper we work with the hypothesis that the coupling between the QD and the leads is maximal, meaning that there are no barriers for electrons entering and leaving the system. In this picture, W becomes independent of any external parameter. This hypothesis is good inasmuch the changes in the confining potential due the periodic perturbation are local and take place far for the QD openings. This means that the distance ℓ between the openings and the perturbed region must be such that $\ell/\lambda_F \gg 1$. Should that not be the case, then $dW/dX \neq 0$, resulting in an additional pumping mechanism similar to that of a classical peristaltic pump, where transport occurs because the constriction are periodically opened and closed while the internal potential is varied. Although the existence of such classical effect in the experiments cannot be entirely ruled out, we do not take it into account in our analysis. The clear existence of mesoscopic, sample-to-sample fluctuations and a marked temperature dependence of the magnitude of the current amplitude in the experiments seems to indicate that the peristaltic effect can be made rather weak. Thus, for a parametrically constant W , we have

$$\frac{\partial S}{\partial X_i} = -2\pi i W^\dagger D^{-1} \frac{\partial H}{\partial X_i} D^{-1} W \quad (7)$$

where $D = E - H(\mathbf{X}) + i\pi W W^\dagger$. Using Eq. (7), it is straightforward to show that $\Pi \equiv \Pi^L = -\Pi^R$.

We are interested in chaotic quantum dots, where the Hamiltonian H can be modeled as a member of one of the Gaussian ensembles of random matrices.¹⁵ For this case, the Hamiltonian matrix elements are assumed uncorrelated but equally distributed. Their variance λ^2/M determines the mean resonance spacing at the center of the band, $\Delta = \pi\lambda/M$. Several studies support that, in

general, the elements of $\partial H/\partial X$ have themselves also Gaussian random entries (see, for instance, Ref. 16 and references therein). We choose their variance to be $(\lambda/MX_c)^2$.¹⁷ In this way, we set the scale of X , making $X = X_c$ correspond to the average parametric change necessary to cause one level crossing. In other words, X_1 and X_2 are measured in units of the average parametric level crossing. Motivated by the fact that pumping currents are usually generated in the presence of an external perpendicular magnetic field that breaks time-reversal symmetry, in what follows we only address the case where H belongs to the unitary ensemble (GUE).

The statistical theory presented above is an alternative to the maximal entropy approach used to calculate the pumping current fluctuations in Refs. 3,10. At $T = 0$ both approaches are equivalent. However, while the maximum entropy has the advantage of leading to analytical expressions for the distribution of Π_0 at $T = 0$, it cannot be consistently extended to finite temperatures.¹⁸ As we show below, temperature plays a very important role in suppressing the pumping current fluctuations.

A. Thermal fluctuations

Let us start addressing the thermal rounding of the Fermi surface, postponing the discussion of dephasing to Sec. IID. The thermal smearing is easily accounted for by the integral

$$I_T(\mu) = \int dE \left(-\frac{\partial f_T}{\partial E} \right) I_0(E), \quad (8)$$

where $f_T = \{\exp[(E - \mu)/T] + 1\}^{-1}$ (we assume $k_B = 1$ hereafter). Hence, the pumping current variance reads

$$\langle I_T^2 \rangle = \left(\frac{e\omega T}{2\pi} \right)^2 \int_{-\infty}^{\infty} d\varepsilon \frac{d}{dT} \left[2T \sinh\left(\frac{\varepsilon}{2T}\right) \right]^{-2} C_0(\varepsilon), \quad (9)$$

where C_0 is the pumping response autocorrelation function at $T = 0$, defined by

$$C_0(\varepsilon) = \int_{\mathcal{A}} dX_1 dX_2 \int_{\mathcal{A}} dY_1 dY_2 D(\varepsilon, \mathbf{X} - \mathbf{Y}) \quad (10)$$

and

$$D(\varepsilon, \mathbf{X} - \mathbf{Y}) = \left\langle \Pi_0 \left(\mu + \frac{\varepsilon}{2}, \mathbf{X} \right) \Pi_0 \left(\mu - \frac{\varepsilon}{2}, \mathbf{Y} \right) \right\rangle. \quad (11)$$

Here $\langle \dots \rangle$ indicates ensemble averaging. If the amplitude of the periodic perturbations is sufficiently weak, such that $\sqrt{\mathcal{A}} \ll X_c$, we can approximate the surface integrals by the mean value of the response function at $X = 0$ times the area, yielding

$$C_0(\varepsilon) \approx \mathcal{A}^2 D(\varepsilon, 0). \quad (12)$$

At very low temperatures, the variance of the pumping current becomes proportional to $C_0(0)$, i.e., $\langle \Pi_0^2 \rangle$. In the

absence of dephasing, we find that Π_0 has zero mean and variance given by (see Appendix A)

$$\text{var } \Pi_0 = \frac{16}{\pi^2} \frac{N_L N_R}{(N^2 - 1)(N^2 - 4)}. \quad (13)$$

Note that $\text{var}(\Pi_0)$ diverges for $N = 2$. As N increases, this divergence is smeared out. For large N , $C_0(\varepsilon)$ quickly tends to a universal, ‘‘semiclassical’’ form. The derivation of this function is presented below.

B. Semiclassical pumping response autocorrelation function

When the number of open channels $N \gg 1$, the pumping response autocorrelation function of Eq. (10) can be directly evaluated using Miller’s semiclassical S -matrix,¹⁹ namely,

$$\tilde{S}_{\alpha\beta}(E, \mathbf{X}) = \sum_{\mu(\alpha \leftarrow \beta)} \sqrt{p_\mu(E, \mathbf{X})} e^{i\sigma_\mu(E, \mathbf{X})/\hbar}, \quad (14)$$

where the classical trajectories that start at channel β and end at channel α are labeled by $\mu(\alpha \leftarrow \beta)$. Accordingly, σ_μ is the reduced action (with a Maslov phase included) and p_μ is the classical transition probability for going from β to α following the path μ . (Quantities indicated by a wide tilde are obtained in the semiclassical approximation.) In the derivation of Eq. (14), the absence of tunneling barriers between the scattering and the asymptotic regions is implicit.

Let us write the pumping response function as $\Pi_0 = \pi^{-1} \sum_\beta \sum_{\alpha \in l} J_{\alpha\beta}$. The semiclassical approximation for $J_{\alpha\beta}$ reads

$$\tilde{J}_{\alpha\beta}(E, \mathbf{X}) = \sum_{\mu, \nu} \frac{\partial \sigma_\mu}{\partial X_1} \frac{\partial \sigma_\nu}{\partial X_2} \sqrt{p_\mu p_\nu} \sin\left(\frac{\sigma_\mu - \sigma_\nu}{\hbar}\right), \quad (15)$$

where μ and ν are trajectories connecting the same pair of two arbitrary channels α and β . The parametric action derivatives are defined as²⁰

$$Q_{i\mu} \equiv \frac{\partial \sigma_\mu}{\partial X_i} = \int_0^{t_\mu} dt \frac{\partial H}{\partial X_i}(\mathbf{p}(t), \mathbf{q}(t), \mathbf{X}), \quad (16)$$

where the integral is evaluated along the trajectory μ over the time t_μ it spends in the QD.

Our ergodic hypothesis is that averages over random matrix ensembles are equivalent to the energy averages taken here. We average $\tilde{J}_{\alpha\beta}(E, \mathbf{X})$ over an energy window δE where the classical dynamics presents little changes, nonetheless fulfilling $\delta E \gg \Delta$. For this task, as customary, we neglect the energy dependence of the probabilities p_μ and keep only contributions from diagonal terms. This approximation is justified for trajectories with dwell times shorter than the Heisenberg time $\tau_H \equiv \hbar/\Delta$, since they are, in general, uncorrelated

for chaotic systems. Fortunately, without barriers, trajectories with t exceeding τ_H are statistically negligible in the semiclassical regime of $N \gg 1$. In the absence of system specific symmetries, the diagonal approximation reads $\langle \exp[i(\sigma_\mu - \sigma_\nu)/\hbar] \rangle_{\delta E} = \delta_{\mu\nu}$. It implies that $\langle \tilde{J}_{\alpha\beta}(E, \mathbf{X}) \rangle_{\delta E} = 0$ and hence $\langle \tilde{\Pi}_0(E, \mathbf{X}) \rangle_{\delta E} = 0$.

We use a similar procedure to obtain the semiclassical pumping response autocorrelation function $\tilde{D}(\varepsilon, \delta \mathbf{X})$, defined as in Eq. (11). Now we deal with a product of two $\tilde{\Pi}_0$ functions evaluated at different energies, $E \pm \varepsilon/2$, and parameter values, $\bar{\mathbf{X}} \pm \delta \mathbf{X}/2$. The actions $\sigma_\mu(E \pm \varepsilon/2, \bar{\mathbf{X}} \pm \delta \mathbf{X}/2)$ are approximated in leading order of classical perturbation theory as

$$\sigma_\mu(E \pm \frac{\varepsilon}{2}, \bar{\mathbf{X}} \pm \frac{\delta \mathbf{X}}{2}) = \sigma_\mu(E, \bar{\mathbf{X}}) \pm t_\mu \frac{\varepsilon}{2} \pm \mathbf{Q}_\mu \cdot \frac{\delta \mathbf{X}}{2}. \quad (17)$$

Let us start examining the J autocorrelation function. The diagonal approximation is used to compute the energy average of $\sin[(\sigma_\mu - \sigma_\nu)/\hbar] \sin[(\sigma_{\mu'} - \sigma_{\nu'})/\hbar]$ and gives

$$\begin{aligned} \langle \tilde{J}_{\alpha\beta}^{(+)} \tilde{J}_{\alpha'\beta'}^{(-)} \rangle_{\delta\varepsilon} &= \frac{1}{2\hbar^4} \text{Re} \sum_{\substack{\mu, \nu (\alpha \leftarrow \beta) \\ \mu', \nu' (\alpha' \leftarrow \beta')}} (\delta_{\nu\nu'} \delta_{\mu\mu'} + \delta_{\nu\mu'} \delta_{\nu'\mu'}) \\ &\times \sqrt{p_\mu p_{\mu'} p_\nu p_{\nu'}} Q_{1\mu} Q_{1\mu'} Q_{2\nu} Q_{2\nu'} \\ &\times \exp \left\{ -\frac{i}{\hbar} \left[\varepsilon(t_\nu - t_\mu) + \delta \mathbf{X} \cdot (\mathbf{Q}_\nu - \mathbf{Q}_\mu) \right] \right\}, \end{aligned} \quad (18)$$

where $J_{\alpha\beta}^{(\pm)} \equiv J_{\alpha\beta}(E \pm \varepsilon/2, \bar{\mathbf{X}} \pm \mathbf{X}/2)$. Since no special attention is paid to time-reversal symmetric paths, Eq. (18) represents the semiclassical correlation function for broken time-reversal symmetry.

We proceed using classical sum rules to convert the sums in Eq. (18) into time integrals. For that purpose, orbits are grouped with respect to common traversal times and averages are taken within these sets. In what follows, we describe the details how this procedure is implemented following two basic steps.

For chaotic systems the transition probabilities p_μ follow the analogue of the Hannay-Ozorio de Almeida sum rule for open systems,²¹

$$\sum_{t \leq t_\mu \leq t + \delta t} p_\mu = \frac{1}{N\tau} e^{-t/\tau} \delta t \equiv \bar{p}(t) \delta t, \quad (19)$$

where $\sum_{t \leq t_\mu \leq t + \delta t} p_\mu$ is the sum of all classical transition probabilities following the trajectories μ belonging to a time interval $[t, t + \delta t]$, where δt is classically small. In Eq. (19), the decay time is $\tau = \hbar/\Gamma$,²² where Γ is the escape width, also known in this context as the Weisskopf S -matrix autocorrelation length.

The transition probabilities p_μ and the parametric action derivatives \mathbf{Q}_μ are uncorrelated. In addition, $Q_{1\mu}$ and $Q_{2\mu}$ are uncorrelated, provided μ dwells inside the QD for a couple traversal times. Thus, for fixed $\bar{\mathbf{X}}$, the time-average in Eq. (19) runs over a large number

of scattering orbits with $\mathbf{Q}_\mu(t)$, which may be considered as samples of the probability distribution $P_t(\mathbf{Q}) = P_t(Q_1)P_t(Q_2)$. The latter is assumed to be Gaussian,²⁰

$$P_t(Q_i) = \frac{1}{\sqrt{2\pi\overline{Q_i^2}(t)}} \exp \left[-\frac{Q_i^2}{2\overline{Q_i^2}(t)} \right]. \quad (20)$$

The Gaussian width is a function of $\bar{\mathbf{X}}$ and \bar{E} , known to grow diffusively with time,²³ namely,

$$\overline{Q_i^2}(t) = \frac{1}{\mathcal{N}(t)} \sum_{t \leq t_\mu \leq t + \delta t} Q_{i\mu}^2 = Bt, \quad (21)$$

where $\mathcal{N}(t)$ is the number of trajectories μ within the time window $[t, t + \delta t]$. The diffusion constant B is not expected to depend on i since both X_1 and X_2 are generic shape parameter. (This is not the case if, for instance, X_1 would stand for a magnetic field and X_2 for a shape deformation.) B is given by

$$B(E, \mathbf{X}) = 2 \int_0^\infty dt \overline{\frac{\partial H}{\partial X}(\mathbf{p}(t), \mathbf{q}(t)) \frac{\partial H}{\partial X}(\mathbf{p}(0), \mathbf{q}(0))}. \quad (22)$$

It is important to notice that the decay of the classical correlation function in Eq. (22) need only be integrable (many available chaotic systems do not exhibit full exponential decay of the correlations). A detailed discussion of the classical properties of \mathbf{Q}_μ and its semiclassical implications for density correlation function can be found in Ref. 20. In particular, there it is shown that X_c is intimately related to the classical diffusion constant, namely, $X_c = (\hbar\Delta/B)^{1/2}/\pi$.¹⁷

By taking the Gaussian average over $\mathbf{Q}_{i\mu}$, inserting (19) and (22) into (18), and integrating over time, we arrive at

$$\tilde{D}(\varepsilon, \delta \mathbf{X}) = \frac{\text{var } \tilde{\Pi}_0}{\left\{ \left(\frac{\varepsilon}{\Gamma} \right)^2 + \left[1 + \frac{2(\delta \mathbf{X})^2}{NX_c^2} \right]^2 \right\}^2}, \quad (23)$$

with

$$\text{var } \tilde{\Pi}_0 = \frac{4}{\pi^2 N^2} \frac{1}{X_c^4}. \quad (24)$$

This expression agrees with the random matrix theory results of Ref. 12, also obtained for $N \gg 1$. The semiclassical $\text{var } \tilde{\Pi}_0$ is also consistent with Eq. (13), as it should.

C. Small- N limit

It is a difficult technical task to calculate an analytical expression for $C_0(\varepsilon)$ in the small- N limit, which is the case of experimental interest. To bridge this gap, we relied on numerical simulations. We typically generated 10^5 members of an ensemble of S matrices defined by Eq. (6), following the prescription given in Ref. 18.

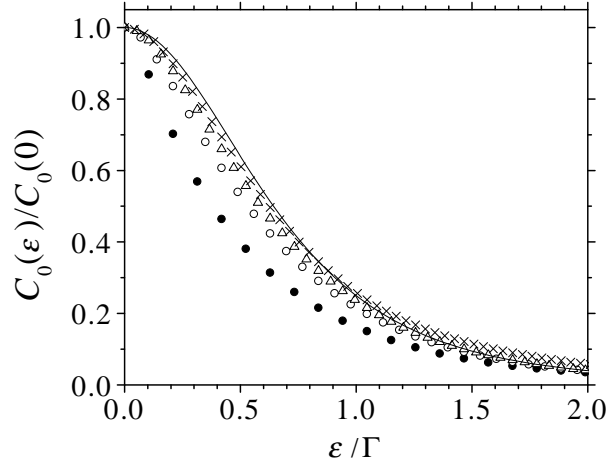


FIG. 1: Pumping current autocorrelation function $C_0(\epsilon)/C_0(0)$ versus energy ϵ in units of Γ . The solid circles represent the $N = N_L + N_R = 4$ case, whereas empty circles, triangle, and crosses stand for $N = 6, 8,$ and 10 , respectively. In all cases $N_L = N_R$. The solid line is the autocorrelation function given by Eq. (23).

The results for $N > 2$ are illustrated by Fig. 1. Notice that as N increases, the semiclassical limit is attained very fast. Nevertheless, for $N = 4$, which is the experimental case in Ref. 5, the depart from the semiclassical limit is still significant. The effect of having a small N is best captured in Fig. 2, where we show the pumping current variance in units of $(e\omega A/2\pi)^2$, namely, $\langle \mathcal{I}^2 \rangle \equiv \langle I_T^2 \rangle / (e\omega A/2\pi)^2$, as a function of temperature. The numerical results were obtained by carrying out the integration in Eq. (9) through an interpolating of the data shown in Fig. 1. We can observe that the fluctuations decrease with increasing temperature and N . In the inset we scaled $\langle \mathcal{I}^2 \rangle$ by $C(0)$ and the temperature by Γ . We observe that while the curves for $N \gtrsim 8$ tends to fall onto each other, the $N = 4$ case shows a marked different behavior.

The limit case of $N = 2$ is special: the variance of the pumping response function Π_0 diverges due to the long tails in the distribution Π_0 .³ Hence, in the absence of dephasing processes, $\langle I_T^2 \rangle$ also diverges. We address this issue in the following subsection.

D. Dephasing

The origin of the quantum pumping current is interference. Thus, the effect is susceptible to dephasing created by the interaction of electrons with phonons, photons, and fluctuations in the electromagnetic environment. While a precise, accessible microscopic theory of dephasing for open quantum pumps is still lacking, some quantitative results can be obtained through phenomeno-

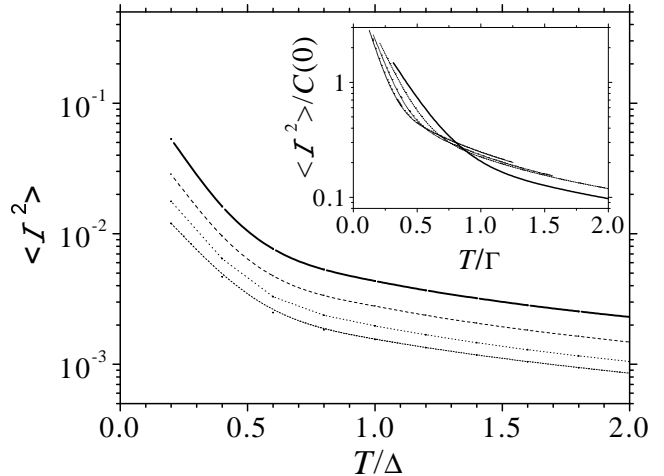


FIG. 2: Pumping current variance $\langle \mathcal{I}^2 \rangle$ in units of $(e\omega A/2\pi)^2$ versus temperature T in units of Δ . The thick solid line stands for the $N = N_L + N_R = 4$ case, whereas dashed, dotted, and short-dashed lines stand for $N = 6, 8,$ and 10 , respectively. In all cases $N_L = N_R$. Inset: Same cases, but for the pumping current variance scaled by $C_0(0)$ (temperature measured in units of Γ).

logical models.^{9,10} In particular, the voltage probe model of Büttiker²⁴ provides a simple way of introducing dephasing by adding a third lead to the QD which neither inject nor drain a net current. Electrons can move in and out of the QD through this lead and loose phase coherence in the process. The amount of dephasing can then be tuned by changing the characteristics of the third lead, such as coupling constant p and number of channels N_ϕ . It is customary to use a single parameter $P_\phi = pN_\phi$ to parametrize the dephasing. We take $N_\phi \gg 1$ and $p \ll 1$, while keeping P_ϕ constant.

Here we adopt the formulation of Ref. 10 and break up the contributions to the pumping current into two parts,

$$I_0^\phi = \frac{\omega e}{2\pi} \int_{\mathcal{A}} dX_1 dX_2 (\Pi_0^{\text{dir}} + \Pi_0^{\text{rec}}). \quad (25)$$

The separation into two components is convenient because Π_0^{dir} becomes Π_0^L [Eq. (5)] as the coupling between the third lead and the QD goes to zero (see below), while Π_0^{rec} disappears in the same limit. The latter represents the contribution to the pumping current coming from a voltage rectification effect (See Sec. III).

Using that $\Pi_0^L + \Pi_0^R + \Pi_0^\phi = 0$ to enforce current conservation (where ϕ denotes the third lead), one finds the relation¹⁰

$$\Pi_0^{\text{dir}} = \frac{G_{R\phi}}{(G_{L\phi} + G_{R\phi})} \Pi_0^L - \frac{G_{L\phi}}{(G_{L\phi} + G_{R\phi})} \Pi_0^R, \quad (26)$$

where $G_{L\phi}$ and $G_{R\phi}$ are the conductances of the QD between the third lead and the left or right leads, respectively. Through steps analogous to those taken to write

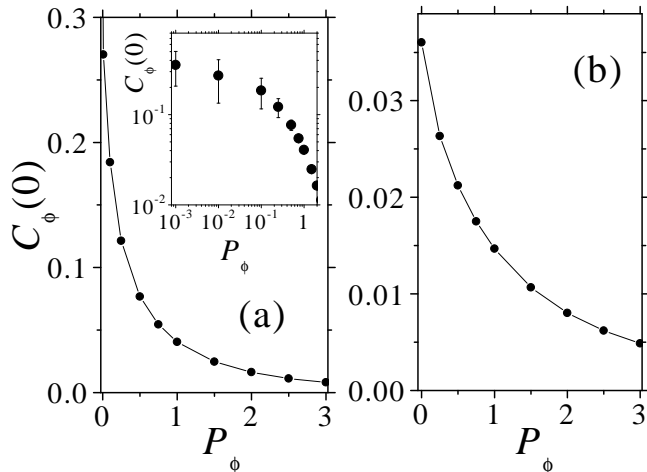


FIG. 3: Pumping response variance $C_\phi(0) = \text{var}(\Pi_\phi)$ as a function of P_ϕ . Solid circles are the result of our numerical simulation (solid lines serve as a guide to the eye). (a) $N = 2$ case. Inset: Same as before, but magnifying the small P_ϕ range (statistical standard deviations shown). (b) $N = 4$ case.

Eqs. (1) to (5), one finds that the rectification current is given by

$$\begin{aligned} \Pi_0^{\text{rect}} = & \frac{1}{4\pi} \sum_{\beta} \sum_{\alpha \in \phi} \text{Im} \left(S_{\alpha\beta}^* \frac{\partial S_{\alpha\beta}}{\partial X_2} \right) \frac{\partial}{\partial X_1} \frac{G_{L\phi} - G_{R\phi}}{G_{L\phi} + G_{R\phi}} \\ & - \frac{1}{4\pi} \sum_{\beta} \sum_{\alpha \in \phi} \text{Im} \left(S_{\alpha\beta}^* \frac{\partial S_{\alpha\beta}}{\partial X_1} \right) \frac{\partial}{\partial X_2} \frac{G_{L\phi} - G_{R\phi}}{G_{L\phi} + G_{R\phi}}. \end{aligned} \quad (27)$$

Below, we study the statistical fluctuations of $\Pi_\phi \equiv \Pi_0^{\text{dir}} + \Pi_0^{\text{rec}}$.

In Fig. 3 we show the effect of dephasing in the pumping response variance, $C_\phi(0) \equiv \text{var}(\Pi_\phi)$, as a function of the dephasing parameter P_ϕ for $N = 2$ and 4. When $N = 2$, the long tails in the distribution of Π_0 make the numerical assessment of $\text{var}(\Pi_\phi)$ increasingly difficult as P_ϕ goes to zero (see inset of Fig. 3a). To investigate this problem, we generated 10^6 realizations of the S matrix for a range of energies E and $P_\phi < 0.1$. We found that the standard deviation increases with the number of realizations; moreover, large values of $|\Pi_\phi|$ were accompanied by abrupt fluctuations of Π_ϕ with E . Upon shrinking the energy steps in our numerical calculations, we found that the number of large fluctuations decreased, but their amplitudes increased. This scaling procedure was computationally very costly; yet, despite the somewhat poor statistics, our results suggest a fractal behavior of Π_ϕ as a function of energy, typical of power-law distributions.²⁵ Therefore, our simulations strongly support that $C_\phi(0)$ diverges for $N = 2$ as $P_\phi \rightarrow 0$, in agreement with Ref. 3. The apparent fractal nature of $\Pi_\phi(E)$ in this case indicates that exchanging the order between thermal and

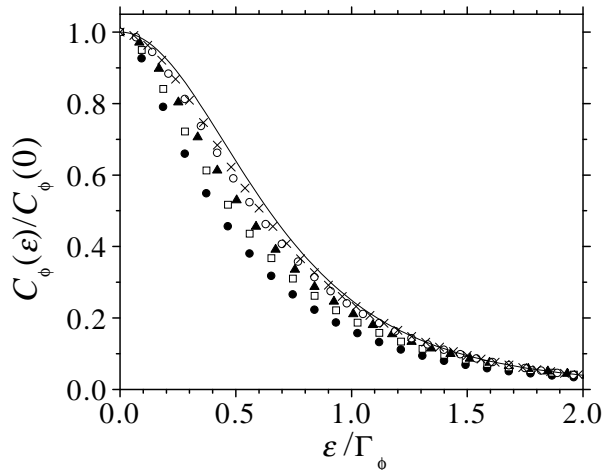


FIG. 4: Normalized pumping response Π_ϕ autocorrelation function $C_\phi(\epsilon)/C_\phi(0)$ versus ϵ/Γ_ϕ for $N_R = N_L = 2$. The solid circles, squares, triangles, empty circles, and crosses stand for $P_\phi = 0.25, 0.5, 1.0, 2.0,$ and 3.0 , respectively. The solid line stands for Eq. (23).

ensemble averages would likely not render a finite value for $\langle I_T^2 \rangle$ either.

For larger values of the dephasing parameter, say $P_\phi \gtrsim 0.1$, we obtained a converged value $\text{var}(\Pi_\phi)$ (small standard deviation) with 10^5 realizations, despite of the very large values of the higher moments. For $P_\phi > 1$, convergence was attained already with 10^4 realizations. We observed (not shown here) that our numerical simulations agree with the analytical results for $C_\phi(0)$ presented in Ref. 10.

In practice, at very low temperatures, $\text{var}(\Pi_\phi)$ is extremely sensitive to small changes in P_ϕ . In this case, although in principle possible, it is very difficult to give a quantitative numerical description of both dephasing and temperature effects. We do not pursue this path here and direct the discussion instead to $N > 2$, where certainly no divergences occur.

A very strong dephasing dependence is absent for $N = 4$. Here, our simulations show that $C_\phi(0)$ remains finite as P_ϕ approaches zero, as depicted by Fig. 3b and in quantitative agreement with Eq. (13). In Fig. 4 we show the effect dephasing in the dimensionless pumping energy autocorrelation function. The correlation function $C_\phi(\epsilon)$ is defined as in Eqs. (11) and (12). We fix $N_R = N_L = 2$ and vary the dephasing parameter P_ϕ . The results represent an average over 10^4 realizations. We find empirically that the energy correlation length scales as

$$\Gamma_\phi = \frac{\Delta}{2\pi} (N + P_\phi). \quad (28)$$

Similarly to the case without dephasing, as P_ϕ increases one quickly reaches the semiclassical regime, characterized by the universal correlation function given by Eq. (23). We verified (not shown here) that our simulations

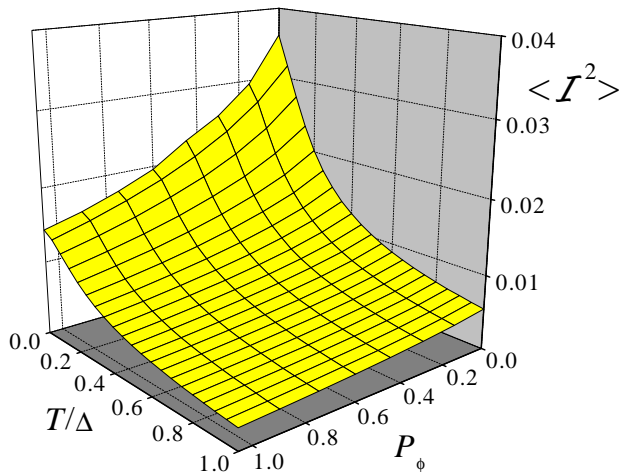


FIG. 5: $\langle \mathcal{I}^2 \rangle$ for $N = 4$ as a function of the temperature and the dephasing strength.

for $C_\phi(0)$ coincide with the analytical results obtained in Ref. 10, as expected.

At this point we can compare the relative role of dephasing and temperature for the pumping current. This is done in Fig. 5, where we display $\langle \mathcal{I}^2 \rangle \equiv \langle I_T^2 \rangle / (e\omega\mathcal{A}/2\pi)^2$ as a function of T and P_ϕ . For $N_R = N_L \geq 2$ we find that, at low temperatures, where typical QDs have for instance $T/\Delta \approx 0.5$ and $P_\phi \approx 0.5$,²⁶ temperature plays a significantly more important role than dephasing. The exception is the remarkable case of $N_R = N_L = 1$ where, in the absence of dephasing, the variance of the pumping current diverges.

III. RECTIFIED CURRENTS

In AlGaAs/GaAs quantum dots formed by lateral electrostatic gates, the rectified component of the dc current tends to dominate over the quantum pumping one at low driving frequencies. This has been recently verified in an experiment where the symmetry properties of induced currents with respect to an external perpendicular magnetic field were studied.²⁷ It was found that while pure quantum pumping currents should be asymmetric with respect to field inversion,¹¹ the actual measured current showed a strong even symmetry, characteristic of rectification.⁶ It is therefore important to characterize the statistical fluctuations of the rectified current as well.

Rectification can arise from two different sources. Firstly, as mentioned in Sec. IID, it appears when inelastic processes take place inside the QD, leading to dephasing. When one models the dephasing process by allowing carriers to move in and out of the QD incoherently through a third lead, an additional reservoir with time-dependent chemical potential, $\mu_\phi(t)$, is required.⁹ Since the time modulation of the QD shape causes the

conductances to vary in time, an incoherent dc current can flow between left and right reservoirs, as long as $G_{L\phi}$ and $G_{R\phi}$ are nonzero. This effect is intrinsic to the QD and has therefore been included in the expression for the quantum pumping current. We remark that the rectified current in this case is also asymmetric with respect to magnetic field inversion.¹⁰ For an open QD, this contribution to the current vanishes as the dephasing strength decreases.

Secondly, rectification also appears due to the capacitive coupling between the shape-deforming electrodes and the left and right reservoirs.^{6,28} The displacement currents and the conductance of the QD oscillate with the same frequency, producing a net dc charge current between the reservoirs. The exact way by which the dc current is induced depends on the particular measurement setup. To illustrate this point, in Fig. 6 we show schematically the two equivalent circuits, namely, for (a) voltage or (b) current measurements.²⁸ Let us briefly derive expressions for the QD voltage and current for these setups, expanding the discussion found in Ref. 6.

(a) *Voltage setup*: in this case the reservoir-QD-reservoir loop is open. Calling $V = V_R - V_L$, with $V_L = 0$, we find that

$$I = C_{2R} \frac{d}{dt} (X_2 - V) + C_{1R} \frac{d}{dt} (X_1 - V). \quad (29)$$

Since $I = GV$ as well, we arrive at

$$V = \frac{1}{G} \left[C_{2R} \frac{d}{dt} (X_2 - V) + C_{1R} \frac{d}{dt} (X_1 - V) \right]. \quad (30)$$

For sufficiently adiabatic pumping (MHz) and small capacitive couplings (pF), we can have $V \ll X_{1,2}$, given that $G^{-1} \leq 26 \text{ K}\Omega$. As a result,⁶

$$V \approx \frac{1}{G} \left(C_{2R} \frac{dX_2}{dt} + C_{1R} \frac{dX_1}{dt} \right). \quad (31)$$

(b) *Current setup*: in this case both reservoirs are grounded and $V_R = 0$. Since $i_g = I - i_{1L} - i_{2L}$, we find

$$I = \frac{V}{R} + C_{2L} \frac{d}{dt} (V - X_2) + C_{1L} \frac{d}{dt} (V - X_1). \quad (32)$$

Using $I = GV$, we get

$$I = \frac{RG}{1 - RG} \left[C_{2L} \frac{d}{dt} (X_1 - V) + C_{1L} \frac{d}{dt} (X_2 - V) \right]. \quad (33)$$

Here we can also neglect V with respect to $X_{1,2}$ on the right-hand side of Eq. (33). Moreover, in the MHz range, where the pumping experiments are carried out, the impedance of the current meter should be smaller than the quantum dot resistance, namely, $RG \lesssim 1$.²⁹ Thus, we finally obtain⁶

$$I \approx RG \left(C_{2L} \frac{dX_1}{dt} + C_{1L} \frac{dX_2}{dt} \right). \quad (34)$$

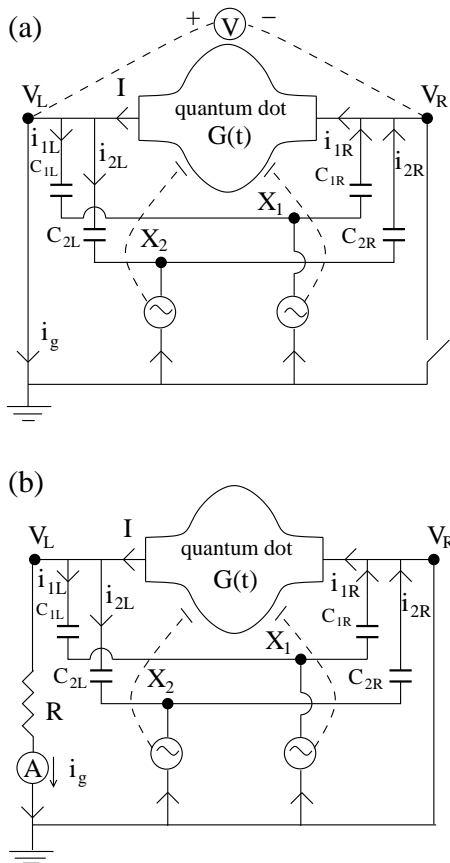


FIG. 6: Equivalent circuits for the quantum pumping measurements: (a) voltage setup; (b) current setup. The electrodes are coupled to the right (left) reservoir through capacitances C_{1R} and C_{2R} (C_{1L} and C_{2L}), with displacement currents i_{1R} and i_{2R} (i_{1L} and i_{2L}). In (a) the reservoir-dot-reservoir circuit is open, while in (b) both reservoirs are grounded. R accounts for the circuit and the current meter internal resistance. X_1 and X_2 are the ac voltages in the electrodes and $G(t)$ is the quantum dot conductance.

Focusing now in the current setup [Eq. (34)], it is straightforward to show that an expression for the rectified current similar to Eq. (4) exists, with the kernel

$$\Pi_0^{\text{cap}} = RC_2 \frac{\partial G}{\partial X_1} - RC_1 \frac{\partial G}{\partial X_2}, \quad (35)$$

where we call $\partial G / \partial X_i$ the parametric conductance velocity with respect to X_i . The statistical fluctuations of this quantity were investigated in Ref. 30, where the distributions of $\partial G / \partial X$ were presented for the $N = 2$ case. Recall that the linear conductance G is given by the Landauer formula

$$G = \frac{e^2}{h} g_0, \quad (36)$$

with the dimensionless conductance at zero temperature defined as

$$g_0 = \sum_{\substack{\alpha \in L \\ \beta \in R}} |S_{\alpha\beta}|^2. \quad (37)$$

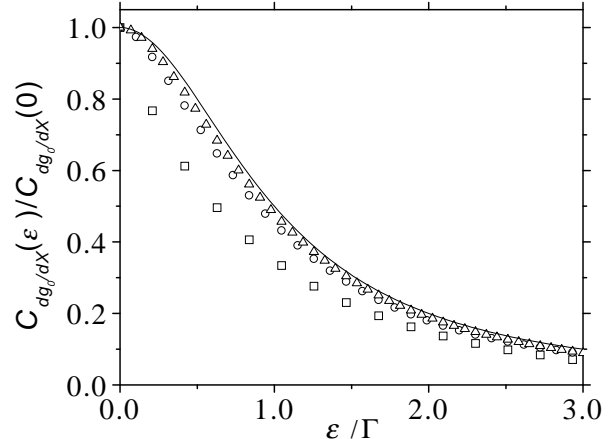


FIG. 7: Parametric conductance velocities autocorrelation function $C_{\partial g_0 / \partial X}(\epsilon)$ as a function of ϵ / Γ . The solid line stands for Eq. (42), while squares, circles, and triangles stand for $N_L = N_R = 1, 2,$ and 3 respectively.

It is difficult to estimate the amplitude of the rectified current derived from Π_0^{cap} , since it depends on R which is unknown. However, the symmetries and statistical properties can be determined and should differ from those of the pure quantum pumping current component. For instance, notice that Π_0^{cap} depends directly on $\partial g_0 / \partial X$. Since the conductance is symmetric with respect to field inversion, and so will be the rectified component of the current in Eq. (34).⁶ Let us focus now on the statistical properties of Π_0^{cap} and on its temperature and dephasing dependences. We argue that thermal smearing plays a key role in suppressing fluctuations of the rectified current as well. In App. C, we study a very closely related issue and show how thermal smearing explains the discrepancy between the recently experimental measured parametric conductance velocity distribution²⁶ and the analytical predictions at zero temperature.³⁰

A simple inspection of Eqs. (6) and (7) shows that $\langle \partial g_0 / \partial X_i \rangle = 0$, since it is proportional to $\langle \partial H / \partial X_i \rangle$. Hence, $\langle \Pi_0^{\text{cap}} \rangle = 0$. The variance of Π_0^{cap} , on the other hand, is given by

$$\text{var}(\Pi_0^{\text{cap}}) = \left(\frac{Re^2}{h} \right)^2 \left[C_2^2 \left\langle \left(\frac{\partial g_0}{\partial X_1} \right)^2 \right\rangle + C_1^2 \left\langle \left(\frac{\partial g_0}{\partial X_2} \right)^2 \right\rangle - 2C_1 C_2 \left\langle \frac{\partial g_0}{\partial X_1} \frac{\partial g_0}{\partial X_2} \right\rangle \right]. \quad (38)$$

For chaotic systems, provided the two parametric perturbations $X_1(t)$ and $X_2(t)$ have the same amplitude, we expect that

$$\left\langle \left(\frac{\partial g_0}{\partial X_1} \right)^2 \right\rangle = \left\langle \left(\frac{\partial g_0}{\partial X_2} \right)^2 \right\rangle \equiv \left\langle \left(\frac{\partial g_0}{\partial X} \right)^2 \right\rangle. \quad (39)$$

If the periodic perturbations X_1 and X_2 are acting at locations far (by several Fermi wavelengths) from each other, it is justifiable to assume that the parametric conductance velocities with respect to different X_i are uncorrelated, $\langle (\partial g_0 / \partial X_1)(\partial g_0 / \partial X_2) \rangle = 0$, leading to $\text{var}(\Pi_0^{\text{cap}}) = R^2(C_1^2 + C_2^2)\langle (\partial g_0 / \partial X)^2 \rangle$. This assumption leads to an analytical expression for the zero-temperature rectified current variance, $\text{var}(i^{\text{rect}})$, in analogy with Eq. (4), since

$$\left\langle \left(\frac{\partial g_0}{\partial X} \right)^2 \right\rangle = \frac{8 N_L^2 N_R^2}{N(N^2 - 1)^2}. \quad (40)$$

[Details on the derivation of Eq. (40) are presented in Appendix B.] In order to compute the temperature dependence of $\text{var}(i^{\text{rect}})$ we need first to calculate the parametric conductance velocity energy autocorrelation function, namely,

$$C_{\partial g_0 / \partial X}(\varepsilon) = \left\langle \frac{\partial g_0}{\partial X} \left(E + \frac{\varepsilon}{2} \right) \frac{\partial g_0}{\partial X} \left(E - \frac{\varepsilon}{2} \right) \right\rangle \quad (41)$$

(recall that $\langle \partial g_0 / \partial X \rangle = 0$). In Fig. 7 we show the results of our simulations for various values of N . Again, as N increases $C_{\partial g_0 / \partial X}(\varepsilon)$ very rapidly converges to

$$C_{\partial g_0 / \partial X}(\varepsilon) = \frac{C_{\partial g_0 / \partial X}(0)}{1 + (\varepsilon/\Gamma)^2}, \quad (42)$$

where $C_{\partial g_0 / \partial X}(0)$ is given by Eq. (40), while deviations are quite large for small N . As in Sec. II C, the thermal fluctuations are enhanced in the small-channel case.

For completeness, let us discuss now the opposite, correlated case, where $\langle (\partial g_0 / \partial X_1)(\partial g_0 / \partial X_2) \rangle = (\partial g_0 / \partial X)^2$. Now $\text{var}(\Pi_0^{\text{cap}}) = R^2(C_1 - C_2)^2 \langle (\partial g_0 / \partial X)^2 \rangle$, making the effect of rectification very small when the capacitive coupling is close to symmetric ($C_1 \approx C_2$). However, it is unlikely that such condition is satisfied in real experimental setups.

Dephasing effects can also be included in Π_0^{cap} phenomenologically by using the voltage probe model in its original form.²⁴ For that purpose, the dimensionless conductance is replaced by

$$g = g_0 + \frac{g_{L\phi} g_{R\phi}}{g_{L\phi} + g_{R\phi}}. \quad (43)$$

We have calculated the distribution of $\partial g_\phi / \partial X$ for several values of N and the dephasing parameter P_ϕ , as introduced in Sec. II D. The conductance velocity autocorrelation function scales in the same way as in the case without dephasing, provided we replace Γ by Γ_ϕ . Results for the case $N = 2$ are shown in Fig. 8. The dependence with P_ϕ is weaker than in the pure quantum pumping case (compare with Fig. 4).

IV. SPIN CURRENTS DUE TO PUMPING AND RECTIFICATION

It was recently pointed out that it is possible to pump a spin current without any net flow of charge through a

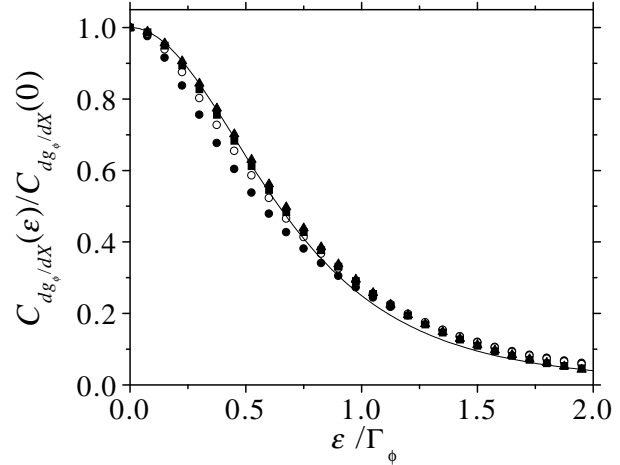


FIG. 8: Parametric conductance velocities autocorrelation function $C_{\partial g_\phi / \partial X}(\varepsilon)$ as a function of ε/Γ_ϕ in the presence of dephasing for $N_L = N_R = 1$. The solid line stands for Eq. (42); squares, circles, triangles, and inverted triangles stand for $P_\phi = 0.5, 1, 2,$ and 4 , respectively.

QD.⁷ The basic idea is to use a parallel magnetic field to Zeeman split resonant states around the Fermi energy. By doing so and tuning the QD shape, one can find a situation where up and down spin components of the pumping current flow in opposite directions. The mechanism by which charge is pumped can be either the ideal quantum pumping of Sec. II or the rectification due to the capacitive coupling between pumping electrodes and reservoirs, as described in Sec. III. A recent experiment has observed the effect.⁸

An important practical question is by how much is the spin current attenuated by dephasing in the orbital (charge) sector of the wavefunctions. Furthermore, it is also interesting to know the amplitude of the effect when the spin pumping current is caused by rectification alone and the number of propagating channels in the leads is not large (both cases had not been considered in the analysis of Ref. 7)

The dependence of the spin current polarization amplitude on the applied parallel field and temperature can be estimated from the correlator $\langle I_\uparrow I_\downarrow \rangle$. Here $I_{\uparrow,\downarrow} = I_T(\mu \pm E_Z/2)$, where $E_Z = g^* \mu_B B_\parallel / 2$ is the Zeeman energy. Using the relations presented in Sec. II, it is straightforward to show that the correlator can be written as

$$\langle I_\uparrow I_\downarrow \rangle = T^2 \int_{-\infty}^{\infty} d\varepsilon \frac{d}{dT} \left[2T \sinh\left(\frac{\varepsilon}{2T}\right) \right]^{-2} C_0(\varepsilon + E_Z). \quad (44)$$

This expression is valid regardless of the nature of the pumping mechanism.

As discussed in Sec. II B, in the case of pure quantum pumping, Eq. (23) provides a semiclassical approximation to the energy correlator in the absence of dephasing

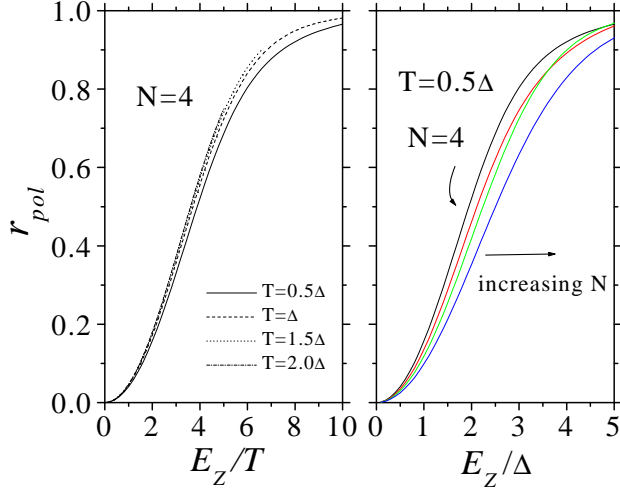


FIG. 9: Spin pumping current polarization coefficient as a function of Zeeman energy E_Z (parallel magnetic field). (a) Curves for different temperatures and a fixed number of channels ($N_R = N_L = 2$). (b) Dependence on the number of channels for a fixed temperature.

and when $N \gg 1$. Using that expression and carrying out simple manipulations, we find that Eq. (44) becomes identical to Eq. (3) of Ref. 7, namely,

$$\langle I_{\uparrow} I_{\downarrow} \rangle = C_0(0) \Gamma \int_0^{\infty} d\tau (1 + \Gamma\tau) e^{-\Gamma\tau} \left[\frac{\pi T \tau}{\sinh(\pi T \tau)} \right]^2 \times \cos(E_Z \tau), \quad (45)$$

The latter was originally derived in Ref. 7 from the linear-response limit of the large- N diagrammatic formalism developed in Ref. 12. Notice that when dephasing is present, Γ has to be replaced by Γ_{ϕ} , as defined in Eq. (28), but the functional dependence on T and E_Z remains the same.

In the small- N limit, we do not have a closed analytical expression for the energy correlator. In this case, the dependence of $\langle I_{\uparrow} I_{\downarrow} \rangle$ on temperature and magnetic field amplitude can only be obtained numerically. Our results for this case are presented in Fig. 9, together with curves derived from Eq. (45). We have opted for plotting the spin current amplitude in terms of the spin polarization coefficient, defined as

$$r_{pol} = \frac{1 - \langle I_{\uparrow} I_{\downarrow} \rangle / \langle I_{\uparrow}^2 \rangle}{1 + \langle I_{\uparrow} I_{\downarrow} \rangle / \langle I_{\uparrow}^2 \rangle}. \quad (46)$$

Notice the rather weak temperature dependence after rescaling the Zeeman energy. In contrast, the dependence on the number of channels is much more pronounced; consequently, a strong dependence on the dephasing parameter P_{ϕ} also occurs. Thus, the same restrictions to orbital (charge) quantum pumping due to decoherence by the environment apply to the spin case.

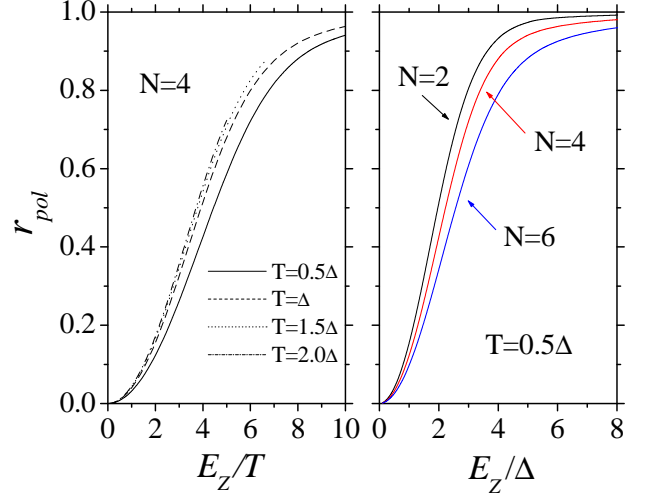


FIG. 10: Same as in Fig. 9, but for rectification-induced spin pumping currents.

Equation (44) is also valid when rectification is present and dominates the pumping mechanism. In this case, in the large- N limit, the energy correlator of Eq. (42) can be used, leading to an expression very similar to Eq. (45), namely,

$$\langle I_{\uparrow} I_{\downarrow} \rangle = 2 C_0(0) \Gamma \int_0^{\infty} d\tau e^{-\Gamma\tau} \left[\frac{\pi T \tau}{\sinh(\pi T \tau)} \right]^2 \cos(E_Z \tau). \quad (47)$$

As in the dissipationless case, here we have to rely on numerical calculations to obtain the correlator in the small- N limit (see Sec. III). Comparative results are shown in Fig. (10) as a function of Zeeman energy (magnetic field) and for different temperatures and number of channels. The curves are very similar to those of Fig. 9. The dependence on temperature is just slightly more pronounced for capacitive pumping. Considering that the energy correlators for the two pumping mechanisms are very similar (a Lorentzian square for pure quantum as opposed to a simple Lorentzian for the capacitive case, in the semiclassical limit), this result comes as now surprise. We conclude that temperature and dephasing dependences alone are not strong indicators of the nature of the pumping mechanism, both for the charge and the spin cases.

V. CONCLUSIONS

In this work we presented numerical (small- N) and semiclassical (large- N) calculations of statistical measures of charge and spin pumping currents in open chaotic quantum dots. Both pure quantum and rectification pumping mechanisms were considered when time-reversal symmetry is broken and the regime is adiabatic. We paid particular attention to the dependences on temperature T , number of propagating channels N , and dephasing.

We were able to draw several conclusions from our results.

Our initial motivation was to propose measuring the damping of pumping current mesoscopic fluctuations as a way to estimate the amount of dephasing present in the experimental setups. However, we found that, for realistic conditions, thermal smearing tends to be a more important effect than dephasing. Lower temperatures are required ($T \ll \Delta$) for dephasing to become quantitative and qualitative distinguishable.

Perhaps one situation where dephasing does have a stronger impact than thermal smearing is when $N = 2$, namely, when there is one single propagating channel in each lead. In this case, dephasing cuts off the divergence of the zero-temperature pure pumping current variance. Taking the thermal average before the ensemble average, on the other hand, does not seem to yield a finite variance when dephasing is absent. In fact, our numerical simulations suggest that the zero-temperature pumping current response function, Π_0 , has a fractal behavior for $N = 2$. A long tail in its probability distribution was observed. Events belonging to this tail were connected to high but isolated peaks in Π_0 as the energy is varied. We observed that such peaks proliferate as the energy increment decreases. Albeit not yet accessible to experimental investigation, a more quantitative understanding of the suppression of this fractal pattern by dephasing is necessary.

We also derived an expression for the pumping response autocorrelation function using the semiclassical approximation in the large- N limit. Our result coincides in the leading order in powers of $1/N$ with that reported in Ref. 11, which was obtained by the diagrammatic technique. The simplicity of the semiclassical derivation relating the pumping current to the instability of the underlying classical orbits provides additional insight to the physical process. In addition, our simulations show that the semiclassical limit is very quickly attained. We also calculated the pumping response variance using the S -matrix maximum entropy approach for pure quantum and rectification pumping. The results are valid for any number of channels and are both consistent with the numerical simulations and with the results presented in Ref. 10.

For the rectification case, we found that the expressions relating the pumping currents and voltages to the driving perturbations are somewhat more involved than that proposed in Ref. 6. Our results only coincide with those of Ref. 6 in the limit of weak capacitive coupling between plunger gates and leads, and when frequencies are not too high (so that the internal impedance of the current meter remains lower than the quantum dot resistance).

Rectification currents induced by capacitive coupling also show mesoscopic fluctuations. However, dephasing effects are less pronounced than for pure quantum pumping. Moreover, the variance does not diverge at zero temperatures for any value of $N \geq 2$.

Pure quantum pumping spin currents have the same characteristics of the charge case. Namely, their variance diverges in the absence of dephasing. We found that increases in temperature, dephasing, or N suppress spin polarization in a similar (strong) way. New mechanisms of pure spin currents generations based on pumping have been proposed recently. Particularly attractive are those based on the spin-orbit coupling present in two-dimensional electron gases formed in III-V heterostructures, which do not require the application of large magnetic fields.^{33,34} For the future, we plan to study how thermal smearing and orbital and spin dephasing affect the magnitude of these new mechanisms.

Acknowledgments

We thank P. Brouwer, G. Finkelstein, C. Marcus, and B. Reulet for useful discussions. MMM is supported by CLAF-CNPq. CHL and ERM acknowledge partial support in Brazil from PRONEX, CNPq, Instituto de Milênio de Nanociências, and FAPERJ. CHL thanks CBPF (Brazil) and the Department of Physics at Duke University for the hospitality. This work was supported in part by NSF Grant No. DMR-0103003.

APPENDIX A: MEAN AND VARIANCE OF THE PUMPING RESPONSE FUNCTION

Here we derive Eq. (13). It is convenient to parametrize the S matrix, its parametric-derivatives, and its energy derivative as

$$S = UV, \quad \frac{\partial S}{\partial X_j} = iUQ_{X_j}V, \quad \text{and} \quad \frac{\partial S}{\partial E} = \frac{2\pi i}{\Delta}UQ_EV, \quad (\text{A1})$$

respectively, for $j = 1, 2$. Here, U and V are $N \times N$ unitary matrices uniformly distributed over the unitary group and independent of Q_{X_j} and Q_E . In turn, the latter are $N \times N$ Hermitian matrices satisfying the joint distribution¹⁰

$$P(S, Q_E, Q_{X_1}, Q_{X_2}) \propto (\det Q_E)^{-9N/2} \times \exp \left\{ -\text{tr} \left[Q_E^{-1} + \frac{1}{8} \sum_{j=1}^2 (Q_E^{-1} Q_{X_j})^2 \right] \right\}. \quad (\text{A2})$$

Also, we parametrize Q_{X_j} as

$$Q_{X_j} = \Psi^{\dagger-1} K_j \Psi^{-1}, \quad (\text{A3})$$

where Ψ is a complex $N \times N$ matrix such that

$$Q_E = \Psi^{\dagger-1} \Psi^{-1} \quad (\text{A4})$$

and K_j is an Hermitian $N \times N$ matrix whose elements are Gaussian distributed with zero mean and variance,

$$\langle K_{ab} K_{a'b'} \rangle = 4(\delta_{ab'} \delta_{ba'} + \delta_{aa'} \delta_{bb'}), \quad (\text{A5})$$

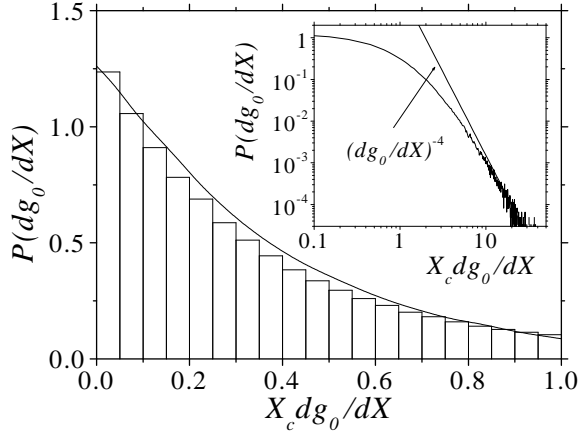


FIG. 11: Distribution of parametric conductance velocities $P(\partial g_0/\partial X)$ for $N = 2$. The histogram is our numerical simulation, whereas the solid line stands for the analytical result of Ref. 30. In the inset we show the tails of the distribution in a log-log scale.

as can be easily seen substituting Eqs. (A3) and (A4) into the distribution (A2).

We substitute Eq. (A1) into Eq. (5) and average over the matrices U, V using the results of Ref. 31. Next, we average over Q_{X_j} using the parametrization of Eq. (A3) and Eq. (A5). As a result, we obtain $\langle \Pi_0 \rangle = 0$ and

$$\text{var } \Pi_0 = -\frac{8N_L N_R}{N(N^2 - 1)} \left[\sum_{a,b,c=1}^N \langle (Q_E^2)_{aa} (Q_E)_{bb} (Q_E)_{cc} \rangle - \sum_{a=1}^N \langle (Q_E^4)_{aa} \rangle \right]. \quad (\text{A6})$$

Now, we write Q_E in its diagonal form as $Q_E = A\hat{\tau}A^\dagger$, where $\hat{\tau}$ is the eigenvalue matrix and A is a random unitary matrix. Substitution of the diagonal form of Q_E into Eq. (A6) gives a result independent of A such that the average over A is easily done. After some algebraic simplifications, we arrive at

$$\text{var}(\Pi_0) = \frac{32N_L N_R}{N+1} [\langle \tau_1^2 \tau_2^2 \rangle + 2\langle \tau_1^3 \tau_2 \rangle + (N-2)\langle \tau_1^2 \tau_2 \tau_3 \rangle]. \quad (\text{A7})$$

Finally, since the dimensionless scape rates $x_n = 1/\tau_n$ are distributed according to the generalized Laguerre ensemble,³²

$$P(x_1, \dots, x_N) \propto \prod_{n < m} (x_n - x_m)^2 \prod_n x_n^N e^{-x_n}. \quad (\text{A8})$$

The averages appearing in Eq. (A7) can be calculated by direct integration. The result is Eq. (13).

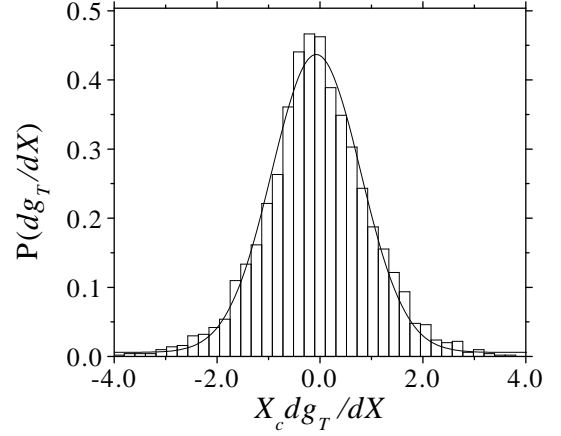


FIG. 12: Distribution of parametric conductance velocities $P(\partial g_T/\partial X)$, $N_R = N_L = 1$, and $T = 0.6\Delta$. The solid line indicates the best Gaussian fit.

APPENDIX B: PARAMETRIC TRANSMISSION COEFFICIENT VELOCITY VARIANCE

In this appendix we show how to obtain $\langle (\partial g_0/\partial X)^2 \rangle$, as given by Eq. (40). As in Appendix A, we find useful to parametrize the S matrix as in Eq. (A1). In this case, Q_X, Q_E , and S have the joint distribution³²

$$P(S, Q_E, Q_X) \propto (\det Q_E)^{-4N} \times \exp \left\{ -\text{tr} \left[Q_E^{-1} + \frac{1}{8} (Q_E^{-1} Q_X)^2 \right] \right\} \quad (\text{B1})$$

We use Eq. (A1) to express $\langle (\partial g_0/\partial X)^2 \rangle$ as a function of U, V, Q_X , and Q_E . With the help of Ref. 31, we average over the matrices U and V . Next, using Eqs. (A3) and (A5), we integrate over Q_X to obtain

$$\left\langle \left(\frac{\partial g_0}{\partial X} \right)^2 \right\rangle = 8 \left[\frac{N_L N_R}{N(N^2 - 1)} \right]^2 \text{Re} \left[-\sum_{a=1}^N \langle (Q_E^2)_{aa} \rangle + N \sum_{a,b=1}^N \langle (Q_E)_{aa} (Q_E)_{bb} \rangle \right]. \quad (\text{B2})$$

Again, we write Q_E in its diagonal form as $Q_E = A\hat{\tau}A^\dagger$ and substitute into Eq. (B2). After some algebra, we arrive at

$$\left\langle \left(\frac{\partial g_0}{\partial X} \right)^2 \right\rangle = \frac{8(N_L N_R)^2}{N(N-1)(N+1)^2} (\langle \tau_1^2 \rangle + N \langle \tau_1 \tau_2 \rangle). \quad (\text{B3})$$

The averages over τ_1^2 and $\tau_1 \tau_2$ can be done explicitly by direct integration using Eq. (A8). The result is Eq. (40).

APPENDIX C: PARAMETRIC CONDUCTANCE VELOCITY DISTRIBUTIONS

This appendix serves to remedy the discrepancy between the theoretical³⁰ and experimental²⁶ distributions of parametric dimensionless velocities $\partial g_0/\partial X$. This discussion gives further support to the statistical theory employed in this paper, and provides a further illustration of the important role of temperature in the statistical fluctuations of conductance-related quantities. In addition, we illustrate the accuracy of the simulations by comparing our results to the theoretical $P(\partial g_0/\partial X)$.

For $N = 2$ the distribution of $\partial g_0/\partial X$ is known for all symmetry classes.³⁰ It shows a singularity at zero derivative: a logarithmic divergence in the presence of time-reversal symmetry ($\beta = 1$) and a cusp in the absence of that symmetry ($\beta = 2$). The tails of $P(\partial g_0/\partial X)$ are algebraic and follow

$$P(\partial g_0/\partial X) \propto (\partial g_0/\partial X)^{-\beta-2}. \quad (\text{C1})$$

In Fig. 11 we show a comparison between our numerical results and the analytical distributions of $\partial g_0/\partial X$.

By numerically convoluting $g_0(\epsilon)$ with the thermal distribution, we obtain g_T . The histogram is shown in Fig. 12 for $T/\Delta = 0.6$, corresponding to the experimental situation in Ref. 26. Notice that even at such low temperatures, T is slightly larger than the $\partial g_0/\partial X$ energy autocorrelation length, suppressing large fluctuations of g_0 at zero temperature and favoring a Gaussian distribution, as observed in the experiment.

The quality of this result suggests that a direct comparison between experimental and theoretical values of $\text{var}(\partial g_T/\partial X)$ can be used to set the scale of the X parameter. The distribution of rectified currents $P(i^{\text{rect}})$ can be obtained straightforwardly from $P(\partial G/\partial X)$.

-
- ¹ D. J. Thouless, Phys. Rev. B **27**, 6083 (1983).
² B. Spivak, F. Zhou, and M. T. Beal Monod, Phys. Rev. B **51**, 13226 (1995).
³ P. W. Brouwer, Phys. Rev. B **58**, R10135 (1998).
⁴ F. Zhou, B. Spivak, and B. Altshuler, Phys. Rev. Lett. **82**, 608 (1999).
⁵ M. Switkes, C. M. Marcus, K. Campman, and A. C. Gosard, Science **283**, 1905 (1999).
⁶ P. W. Brouwer, Phys. Rev. B **63**, 121303(R) (2001).
⁷ E. R. Mucciolo, C. Chamon, and C. M. Marcus, Phys. Rev. Lett. **89**, 146802 (2002).
⁸ S. K. Watson, R. M. Potok, C. M. Marcus, and V. Umansky, preprint (cond-mat/0302492).
⁹ M. Moskalets and M. Büttiker, Phys. Rev. B **64**, 201305(R) (2001).
¹⁰ J. N. H. J. Cremers and P. W. Brouwer, Phys. Rev. B **65**, 115333 (2002).
¹¹ T. A. Shutenko, I. L. Aleiner, and B. L. Altshuler, Phys. Rev. B **61**, 10366 (2000).
¹² M. G. Vavilov, V. Ambegaokar, and I. L. Aleiner, Phys. Rev. B **63**, 195313 (2001).
¹³ M. Büttiker, H. Thomas, and A. Prêtre, Z. Phys. B **94**, 133 (1994).
¹⁴ C. Mahaux and H. A. Weidenmüller, *Shell-Model Approach to Nuclear Reactions* (North-Holland, Amsterdam, 1969).
¹⁵ M. L. Mehta, *Random Matrices*, 2nd ed. (Academic Press, San Diego, 1991).
¹⁶ M. Barth, U. Kuhl, and H.-J. Stöckmann, Phys. Rev. Lett. **82**, 2026 (1999).
¹⁷ We chose X_c to agree with other pumping studies. However, notice that $X_c^{\text{usual}} = \pi X_c$ is customarily found in the literature instead.
¹⁸ E. R. P. Alves and C. H. Lewenkopf, Phys. Rev. Lett. **88**, 256805 (2002).
¹⁹ W. H. Miller, Adv. Chem. Phys. **30**, 77 (1975).
²⁰ A. M. Ozorio de Almeida, C. H. Lewenkopf, and E. R. Mucciolo, Phys. Rev. E **58**, 5693 (1998).
²¹ L. P. Kadanoff and C. Tang, Proc. Natl. Acad. Sci. USA **81**, 1276 (1984); J. H. Hannay and A. M. Ozorio de Almeida, J. Phys. A **17**, 3429 (1984).
²² R. O. Vallejos and C. H. Lewenkopf, J. Phys. A **34**, 2713 (2001).
²³ J. Goldberg, U. Smilansky, M. V. Berry, W. Schweizer, G. Wunner, and G. Zeller, Nonlinearity **4**, 1 (1991).
²⁴ M. Büttiker, Phys. Rev. B **33**, 3020 (1986).
²⁵ B. Hückestein, R. Ketzmerick, and C. H. Lewenkopf, Phys. Rev. Lett. **84**, 5504 (2000).
²⁶ A. G. Huibers, S. R. Patel, C. M. Marcus, P. W. Brouwer, C. I. Duruöz, and J. S. Harris, Jr., Phys. Rev. Lett. **81**, 1917 (1998).
²⁷ L. DiCarlo, C. M. Marcus, and J. S. Harris, preprint (cond-mat/0304397).
²⁸ M. Switkes, Ph.D. thesis, Stanford University (1999).
²⁹ C. M. Marcus (private communication).
³⁰ P. W. Brouwer, S. A. van Langen, K. M. Frahm, M. Büttiker, and C. W. J. Beenakker, Phys. Rev. Lett. **79**, 913 (1997).
³¹ P. A. Mello, J. Phys. A. **23**, 4061 (1990).
³² P. W. Brouwer, K. M. Frahm and C. W. J. Beenakker, Phys. Rev. Lett. **78**, 4737 (1997).
³³ M. Governale, F. Taddei, and R. Fazio, preprint (cond-mat/0211211).
³⁴ P. Sharma and B. W. Brouwer, preprint (cond-mat/0306001).